

OM2S2: On-Line Moisture-Sensing System Using Multifrequency Microwave Signals Optimized by a Two-Stage Frequency Selection Framework

Jinyang Zhang^{ID}, Student Member, IEEE, Yin Bao^{ID}, Dongdong Du^{ID}, Jun Wang^{ID}, and Zhenbo Wei^{ID}, Member, IEEE

Abstract—In this article, an on-line microwave moisture sensing system (OM2S2) based on a multifrequency swept technique was developed to monitor the moisture content (MC) of corn in the fresh to dry state (MC ranged from 10.89 to 63.64%) in real time. Attenuation and phase shift data were collected under a frequency swept signal containing 801 frequencies from 2.00 to 10.00 GHz with a 10 MHz interval. To remove the inefficient frequencies, the optimized frequencies were selected by a two-stage frequency selection framework: 1) 17 frequency subsets were generated using the random forest-recursive feature elimination algorithm, and then 2) the optimal frequency set (including eight individual frequencies) was determined using voting strategies according to the results of tenfold cross-validation. The attenuation and phase shift data corresponding to the optimal frequency set were utilized as the input variables of six regression algorithms for MC prediction. A deep neural network (coefficient of determination(R^2) = 0.997, root mean square error (RMSE) = 1.087, mean absolute error (MAE) = 0.868) performed best according to the Friedman test and Nemenyi *post hoc* test and thus, was employed for the OM2S2. These results showed that the OM2S2 could measure the MC of corn changing from the fresh state to the dry state in real time, and it showed potential for utilization in the on-line determination of high MC in food processing and agriculture-related industries.

Index Terms—Deep neural network (DNN), frequency selection, moisture content, multifrequency swept signal, on-line measurement.

Manuscript received June 6, 2020; revised September 14, 2020; accepted October 12, 2020. Date of publication October 27, 2020; date of current version July 19, 2021. This work was supported by the National Key Research and Development Program of China under Project 2016YFD070190402. (Corresponding author: Jinyang Zhang; Zhenbo Wei.)

Jinyang Zhang, Dongdong Du, Jun Wang, and Zhenbo Wei are with the Department of Biosystems Engineering, Zhejiang University, Hangzhou 310058, China (e-mail: zhangjinyang@zju.edu.cn; dudd@zju.edu.cn; jwang@zju.edu.cn; weizhb@zju.edu.cn).

Yin Bao is with the Department of Biosystems Engineering, Auburn University, Auburn, AL 36830 USA (e-mail: yzb0016@auburn.edu).

Color versions of one or more of the figures in this article are available online at <https://ieeexplore.ieee.org>.

Digital Object Identifier 10.1109/TIE.2020.3032927

I. INTRODUCTION

MOISTURE content (MC) is a very important indicator to assess the quality of a product and its optimal handling and processing conditions. Highly automated industrial processes in food processing and agriculture-related industries require the development of equipment for continuous measurement and monitoring of MC of agricultural and food products [1]–[3]. Since conventional direct measurement techniques for moisture determination, such as oven drying and Karl Fisher titration, are destructive and time-consuming [4], they are not practical for on-line measurement. In some research, capacitance [5] and near-infrared (NIR) methods [6] have been employed to measure the moisture content of agricultural materials in real time. However, the capacitance method is not a perfect solution for on-line measurement because the capacitive sensor takes time to introduce samples between the electrodes [7]. NIR sensor systems can only measure at a small area on the surface of the sample (penetration depths in the μm -range). Since the internal moisture and surface moisture are inconsistent for general agricultural products, especially those with high MC, the NIR measurement results have poor representativeness [8], [9]. As mentioned above, due to the absence of effective methods and techniques that apply to high level of moisture content, it is an urgent need and a significant challenge to develop equipment that can accurately measure the moisture content of high-MC agro-products in real time.

The microwave method is an indirect moisture determination method based on the interaction between microwaves and water molecules in agro-products. It has the advantages of being nondestructive and quick, so it can be used on products in production line. Moreover, microwaves penetrate orders of magnitude deeper than NIR radiation and measure volumes of the samples, thereby yielding more representative results [10], [11]. Microwave methods can be categorized as near-field measurement methods, transmission-line methods, resonant cavity methods, and free-space transmission measurement methods [12]. The free-space transmission measurement is nondestructive and contactless, so it is an ideal way to realize on-line measurement, and it has been applied to measure the MC of cereal grain online [1], [13].

In the past studies, the measurement range of moisture content is limited and at a low level. Much research has focused on establishing a calibration function that can describe the relationship between the microwave characteristics and the MC of the sample, but the measurement equipment calibrated using these functions failed in the high MC range [14]. Meanwhile, a variety of individual frequencies were applied to the free-space transmission measurement to determine the moisture content of agricultural materials, e.g., 4.9, 5.8, 10, and 14.2 GHz [4], [11], [15]. However, the reasons for choosing these frequencies were not explained clearly in the literature. Given that agricultural products are composed of different chemical substances that exhibit different effects on the transmission characteristics of microwaves, it may not be a good practice to measure the MC of different agro products based on one certain frequency [16].

Recent studies have shown that the application of multifrequency measurements can help to expand the measurement range [8], [9], [17]. For general agricultural materials, the behavior of the dielectric constant ϵ' is regular with respect to the frequency (ϵ' decreases with increasing frequency), but the variation of the dielectric loss factor ϵ'' is much less regular owing to the influence of dielectric relaxation and conduction processes [13]. Therefore, the microwave characteristics, such as attenuation and phase shift, obtained at different frequencies are not linearly related to each other. This means that the multifrequency measurement will produce more MC-relevant information, which will reduce the uncertainty in the estimation of the MC of an unknown sample [18], [19]. Therefore, a novel on-line microwave moisture sensing system (OM2S2) innovatively introduces the multifrequency swept technique to acquire extensive feature data (attenuation and phase shift data) to deal with high-MC agro products.

However, although the application of the multifrequency swept technique can collect various useful MC-relevant information, it also collects much redundant information by some ineffective frequencies. Therefore, it is critical to optimize the frequency swept signal and select the most efficient frequencies for high-MC measurements. In this study, a two-stage frequency selection framework (FSF) was presented to optimize the frequency swept signal. The FSF was established as follows: 1) Random forest–recursive feature elimination (RF-RFE) was applied to generate candidate frequency sets; then, 2) the majority voting method (MVM) was adopted to determine the final optimal frequency set.

The attenuation and phase shift data obtained under the optimal frequency set were taken as the input variables of the deep neural network (DNN) algorithm to evaluate the complex interactions between microwave and moist materials [20], [21]. We attempt to build an Adaptive-DNN, which will automatically change the net topology when dealing with different frequency swept data. An adaptive module will be designed in the DNN to dynamically change the number of neurons in the hidden layer according to the number of input features. Two regularization techniques (dropout and early stopping) will be used to reduce overfitting in DNN, and batch normalization is used to speed up the training of the DNN model. The Friedman test and the Nemenyi *post hoc* test were applied to distinguish the DNN

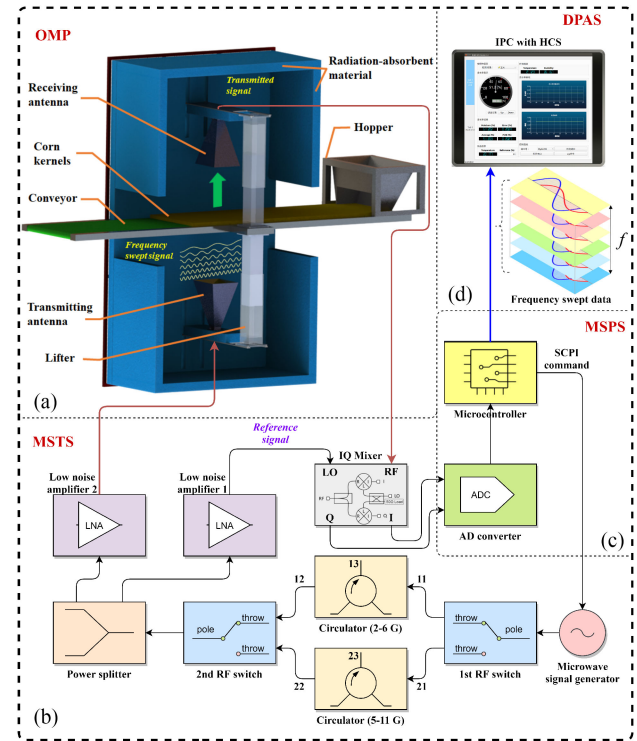


Fig. 1. Schematic diagram of the on-line microwave moisture sensing system (OM2S2). a) On-line measurement platform (OMP). b) Microwave signal transceiver system (MSTS). c) Microwave signal processing system (MSPS). d) Data processing and analysis system (DPAS).

model and models trained by other mainstream algorithms and then deploy the bestfitting regression model to the OM2S2.

In general, very limited optimization work has been carried out on realizing the on-line measurement of the high-MC of agricultural and food products. In this context, the aims of the present study are: 1) To develop an on-line moisture-sensing system that can measure the moisture content of materials with high MC, 2) to present a frequency selection framework to determine the optimal measurement frequency according to experimental object, and 3) to develop an effective MC prediction model by comparing different regression algorithms.

II. ON-LINE MICROWAVE MOISTURE SENSING SYSTEM

A. Structure and Composition of OM2S2

A schematic diagram of the on-line microwave moisture sensing system is shown in Fig. 1. The OM2S2 consists of four subsystems, namely an on-line measurement platform, microwave signal transceiver system (MSTS), microwave signal processing system (MSPS), and data processing and analysis system. The on-line measurement platform contains an anechoic chamber made of radiation-absorbent materials to prevent unwanted reflections that may interfere with the measurements, providing a clean electromagnetic environment for online measurement. The MSTS generates the frequency swept signal and receives the transmitted signal that passes through the sample. The MSPS collects the frequency swept data (attenuation and phase shift of microwave at various frequencies) and uploads them to the

data processing and analysis system, which stores the frequency swept data and calls the moisture prediction model to calculate the sample's MC in real time. The MSTS is the key part of the OM2S2; its composition is described in detail in the following section.

As shown in Fig. 1(b), the microwave signal generator (DS INSTRUMENTS, SG24000H) is connected to the first radio-frequency (RF) switch, which routes microwave signals through different circulators. The SG24000H has the features of a wide frequency range (0.06–24 GHz) and significantly low phase noise (<-93 dBc). The MSTS combines two circulators operating in different bands, so that it can operate at 2–10 GHz. The power splitter divides the microwave signal output by the second RF switch into two equal parts. One part is sent to the local oscillator (LO) port of the IQ mixer as the reference signal after amplification by the first low noise amplifier (LNA). The other part is radiated to the sample as the incident signal through the transmitting antenna (HENGDA MICROWAVE, Model HD-2010DRHA10NZJG) after amplification by the second LNA. Facing the transmitting antenna is the receiving antenna (HENGDA MICROWAVE, Model HD-2010DRHA10NZJG), which collects the radiation transmitted through the sample. The two broadband horn antennas (operating at 2 to 10 GHz) were 1720-mm apart with a far-field setup, and the distance from the transmitting antenna to corn is the same as the distance from the receiving antenna to corn. The transmitted signal is sent to the RF port of the IQ mixer. The analog-to-digital (AD) converter collects the output data from the IQ mixer and uploads them to an industrial personal computer (IPC). The host computer software running on the IPC stored these data and called the moisture prediction model to calculate the MC of the sample. The results are shown on the GUI of the host computer software.

B. Measurement of Attenuation and Phase Shift

The dielectric properties of a material describe its polarization status when it is subjected to an electric field, and water is the most influential factor on the dielectric properties of materials owing to its polar nature [10], [22]. Thus, the MC of materials can be determined by measuring their dielectric properties or parameters related to that [11], such as the attenuation and phase shift of the microwave [9]. In this study, the attenuation and phase shift of microwave signals were extracted from the output signal of the IQ mixer. In the IQ mixer, the RF input was divided into two paths. In the first path, the RF input is mixed with the LO signal and provided the in-phase (I) signal. In the second path, the RF signal was mixed with the 90° phase-shifted LO signal and provided the quadrature (Q) signal. As shown in Fig. 1(b), the reference signal and the transmitted signal were sent to the LO and RF ports of the IQ mixer, respectively. Because the scattering matrices of the in-phase power divider and the quadrature hybrid in the IQ mixer are known, the characteristics of the reference signal and the transmitted signal can be derived from the I and Q signals. Because the reference and transmitted signals have the same frequency, the voltage of the I and Q signals, denoted as V_I and V_Q , have dc values and can be expressed as follows:

$$V_I = \frac{K}{4} V_{LO} V_{RF} \cos \phi \quad (1)$$

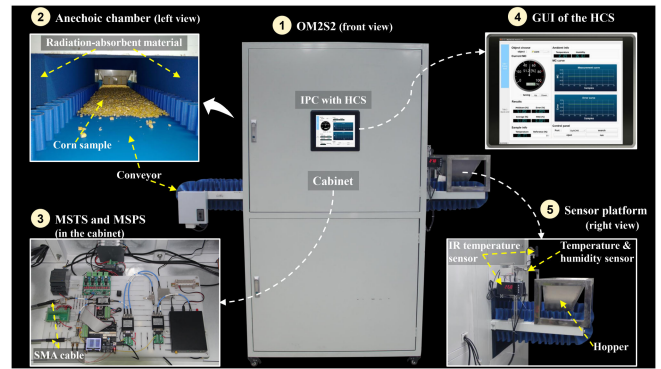


Fig. 2. Experimental setup for the on-line measurement of moisture content. 1) On-line microwave moisture sensing system (OM2S2). 2) Anechoic chamber and corn sample. 3) Microwave signal transceiver system (MSTS) and microwave signal processing system (MSPS). 4) Host computer software (HCS) for collecting experimental data and displaying the measurement results of moisture content. 5) Sensor platform for monitoring the temperature of the sample, ambient temperature, and relative humidity.

$$V_Q = \frac{K}{4} V_{LO} V_{RF} \sin \phi \quad (2)$$

$$P_{RF}(\text{dBm}) = L_c(\text{dB})$$

$$+ 10 \log \left\{ \frac{[V_I(\text{mv})]^2 + [V_Q(\text{mv})]^2}{2R} \times 10^{-3} \right\} \quad (3)$$

$$\phi = \arctan \left(\frac{V_Q}{V_I} \right) \quad (4)$$

where K is a constant accounting for the voltage conversion loss of the mixer, V_{LO} is the amplitude of the LO signal, V_{RF} is the amplitude of the RF signal, ϕ is the phase angle between the RF and LO signals, P_{RF} is the power level at the RF port, and L_c is the conversion loss of the IQ mixer.

The attenuation A is the difference between the power levels without sample ($P_{RF, No-load}$) and with the sample ($P_{RF, Sample}$) placed between the transmitting and receiving antennas, and the phase shift $\Delta\phi$ is the difference between the phase measured without the sample ($\phi_{No-load}$) and with the sample (ϕ_{Sample}). Hence, using (1)–(4), A and $\Delta\phi$ can be expressed as follows:

$$A(\text{dB}) = P_{RF, Sample}(\text{dBm}) - P_{RF, No-load}(\text{dBm}) \quad (5)$$

$$\Delta\phi(\text{rad}) = (\phi_{Sample} - \phi_{No-load}) - 2\pi n \quad (6)$$

where n is an integer that can be obtained by selecting a thickness for an expected permittivity range [23]. On the whole, the moisture-sensing system is employed for collecting the frequency swept data which is used as feature data to build moisture prediction model.

C. Experimental Setup for On-Line Measurement of MC

Fig. 2 shows a schematic of the experimental setup of the on-line measurement of the MC. Since the temperature of the material and the conditions of the experimental environment affect the interaction between microwaves and moist materials, a sensor platform was developed to monitor the temperature of samples,

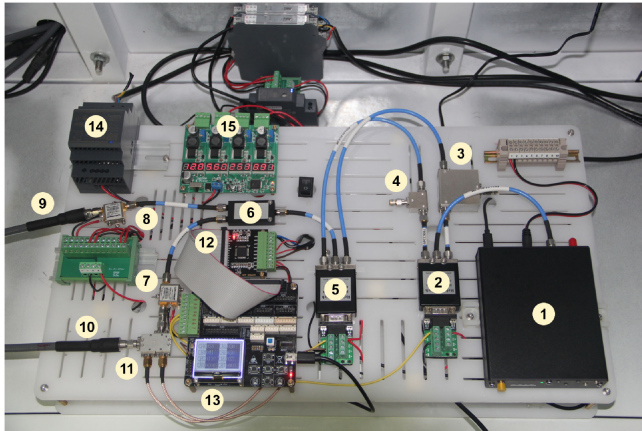


Fig. 3. Microwave circuit of the microwave signal transceiver system (MSTS) and microwave signal processing system (MSPS). (1) Microwave signal generator. (2) 1st RF switch. (3) Circulator (2–6 GHz). (4) Circulator (5–11 GHz). (5) 2nd RF switch. (6) Power splitter. (7) LNA 1. (8) LNA 2 (9) Cable to transmitting antenna. (10) Cable from receiving antenna. (11) IQ mixer. (12) AD converter. (13) Microcontroller. (14) 24-V power supply. (15) 4-channel switching power supply module.

ambient temperature, and relative humidity during the measurement to ensure consistency. The MSTS and MSPS were placed in the cabinet in the OM2S2 to shield against external interference; as the MSTS and MSPS interact closely, they were fixed on the same base. Fig. 3 shows the microwave circuit of the MSTS and MSPS setup. It can be seen that the MSTS is connected to the on-line measurement platform through two SMA cables. In addition, the IPC is embedded on the surface of the OM2S2 cabinet with a user-friendly position. The experiment in Section III-B was carried out based on the above experimental setup.

III. EXPERIMENTAL

A. Preparation of Samples With Different Moisture Content

The corn used throughout this experiment was “Hua Liang 78” variety, which was supplied by Super Green Farm Company. The corn was harvested in September 2019 in Binzhou, Shandong province, China (117.58 E, 37.22 N). To be consistent with the actual situation, corn samples with different moisture content were obtained by natural air drying instead of any heating method. First, all the fresh ears of corn were peeled and then placed in a dry and ventilated environment. In each group of experiments, a specified number of corn ears were taken out and placed in the laboratory (22 °C) for 30 min to allow temperature equilibrium. Then, the corn ears were threshed to provide corn kernels in the multifrequency swept measurement. Since the corn is a raw material for corn flour products and fresh corn products, this study investigated 40 batches of samples with moisture content between that of dried corn (10.89% w.b.) and that of fresh corn (63.64% w.b.).

B. Multifrequency Swept Measurements

During the measurement (with the set up shown in Fig. 2), the moisture-sensing system generated a frequency swept signal

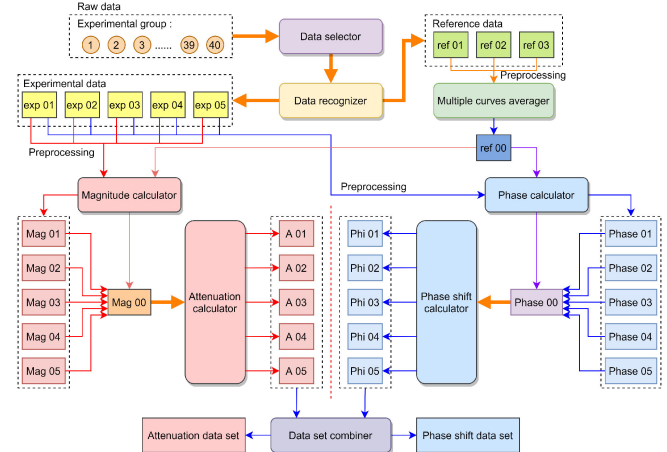


Fig. 4. Execution logic of the data collation program. In the program, the developed data selector and data recognizer take out the reference data *ref 01–ref 03* (measured without the sample) and the experimental data *exp 01–exp 05* (measured with the sample) collected from samples with the same moisture content. Attenuation *A 01–A 05* and phase shift *Phi 01–Phi 05* are determined by the attenuation calculator and the phase shift calculator by comparing the average reference data *ref 00* to the experimental data *exp 01–exp 05*. The dataset combiner collates the attenuation and phase shift data obtained from the samples with different moisture content into an attenuation dataset and a phase shift dataset.

containing 801 frequencies from 2.00 to 10.00 GHz with a 10-MHz interval. Initially, there were no samples on the conveyor to register the initial voltages which provide the references for attenuation and phase, and the no-load measurements were carried out three times to obtain three sets of reference data. Then, corn kernels were loaded into the hopper and sent to the measurement space by the conveyor to acquire experimental data. While microwaves penetrated the sample successively, the feature data on the microwave attenuation and phase shift were sequentially recorded. Finally, the position of the sample was changed by the conveyor for the next measurement, and five repeated measurements were performed at this moisture level.

After collecting the experimental data, a small portion of the sample was taken to determine the true MC of the sample using the oven-drying method in which samples of 30 g in triplicates were dried at 103 °C for 6 h [24]. Subsequently, a new batch of corn ears was taken out and threshed, and the multifrequency swept measurements were carried out at a different MC level. Finally, 200 measurements were taken at 40 MC levels at 22 °C. A data collation program (DCP) was developed to collate the raw data collected in the experiments, and the execution logic of the DCP is illustrated in Fig. 4.

IV. RESULTS AND DISCUSSION

A. Microwave Spectrum Analysis

Fig. 5 shows the attenuation spectrum of corn samples with MCs from 11.00 to 63.64% w.b. As shown in Fig. 5(b), the microwave attenuation varies slightly with frequency with range (maximum–minimum) all less than 16 dB for corn samples with

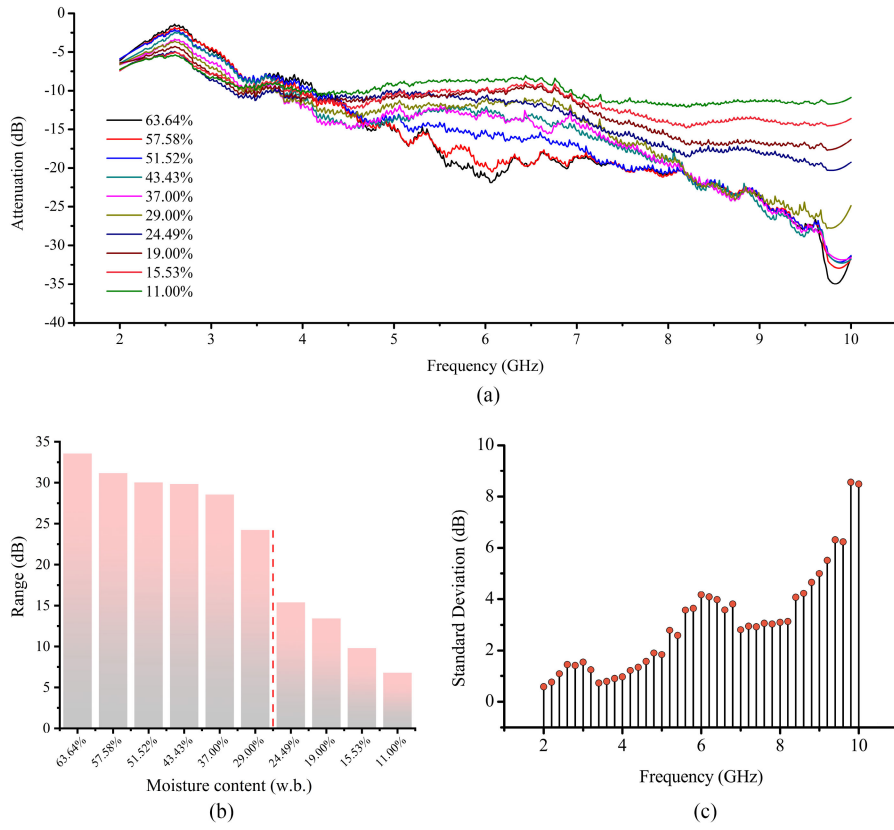


Fig. 5. Microwave spectrum analysis. (a) Original microwave responses obtained from the samples with different moisture content. (b) Range of each microwave spectrum. (c) Standard deviation of attenuation values at different frequency bands.

MC lower than 29.00% w.b. However, the microwave attenuation changes sharply with frequency for corn samples with MC higher than 29.00% w.b., with range all greater than 24 dB. This indicates that the dependencies between the measurement frequency and signal attenuation are significantly different for the low-MC and high-MC samples. Therefore, it is necessary to pay more attention to the selection of the measurement frequency, especially for high-MC samples.

In addition, the differences between these spectra varies greatly in different frequency bands. As shown in Fig. 5(a), the spectrum distribution is very irregular around 4 GHz, while the spectrum distribution is relatively scattered around 6 GHz. To gain more insight, the standard deviation (SD) of attenuation values at different frequency bands was calculated to quantitatively describe the degree of convergence of these spectra. As shown in Fig. 5(c), the SD value at some frequency bands is very small (e.g., around 4 GHz). This means that samples with significantly different MCs have similar attenuation values at such frequency bands. Thus, it is impossible to distinguish the MC of different samples according to the attenuation values measured at those frequencies. Therefore, such frequencies are not appropriate as the measurement frequency. As an example, Fig. 6 presents the microwave attenuation and phase shift for different MCs at 3.50 and 6.00 GHz. As shown in Fig. 6, the attenuation and phase shift of microwave at 6.00 GHz are more sensitive to the change in MC than those of at 3.50 GHz. Therefore, it is necessary to optimize the measurement frequency.

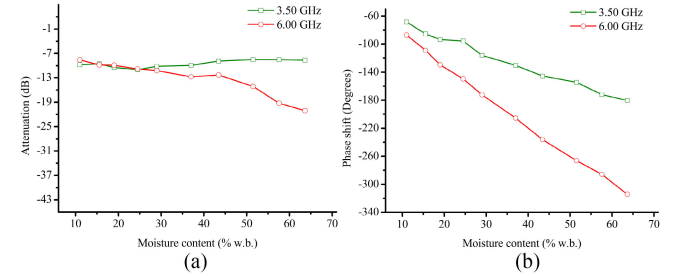


Fig. 6. Variation of attenuation and phase shift of microwave at 3.50 and 6.00 GHz with moisture content.

B. Optimization of Measurement Frequency

1) Frequency Selection Framework Based on RF-RFE:

Recursive feature elimination (RFE) is commonly used together with some pattern recognition algorithms for feature selection [25], [26]. The random forest (RF) algorithm can effectively handle high-dimensional data, such as the frequency swept data [27], and can provide a ranking of the importance of features according to their regression contribution [28]. Thus, a frequency selection framework (FSF) based on the RF-RFE algorithm was proposed to determine the optimal frequency set in this study. As shown in Fig. 7, the frequency selection process includes two stages: 1) The RF-RFE algorithm is used to generate candidate frequency subsets, and then 2) the majority voting

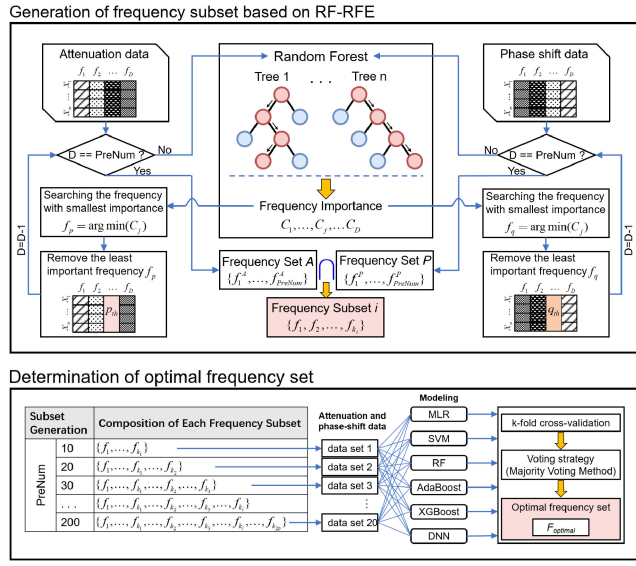


Fig. 7. Structure of the proposed two-stage frequency selection framework. Stage I: The RF-RFE algorithm is employed to generate candidate frequency subsets. Stage II: The majority voting method (MVM) is employed to select the optimal frequency set from the candidate frequency subsets generated at Stage I according to the results of cross-validation.

method (MVM) is used to determine the optimal frequency set according to the results of cross-validation.

In the first stage, the RF algorithm was used to train the model based on the training data from the attenuation or phase shift datasets and determine the importance of the features corresponding to each frequency. Then, the frequencies were ranked by feature importance. Finally, the least important frequency was removed, and then the updated feature data was used to retrain the RF model. This procedure was iterated until a preset number of frequencies remained. However, with no prior knowledge of this preset number (PreNum), the selection of the final subset is often ambiguous and subjective [25], [28]. Therefore, the PreNum was regarded as a hyperparameter and a grid search from 10 to 200 was conducted in the FSF to determine it. In each search process, Frequency Set A and Frequency Set P were obtained from the attenuation and the phase shift datasets by the RF-RFE algorithm, respectively. The intersection of the two sets was used as the final frequency subset, and the corresponding feature dataset was extracted from the original dataset according to this frequency subset.

In the second stage, six algorithms were employed and compared, namely, multiple linear regression (MLR), support vector machine (SVM), random forest (RF), adaptive boosting (AdaBoost), extreme gradient boosting (XGBoost), and deep neural network (DNN). These algorithms were used to establish MC prediction models based on the extracted feature dataset corresponding to each frequency subset. Tenfold cross-validation was applied to evaluate the performance of the regression models. Because the MVM is simple for implementation, effective in decision-making, and appropriate in single-winner applications [29], the FSF uses MVM to determine the optimal frequency set according to the performance measures obtained by cross-validation.

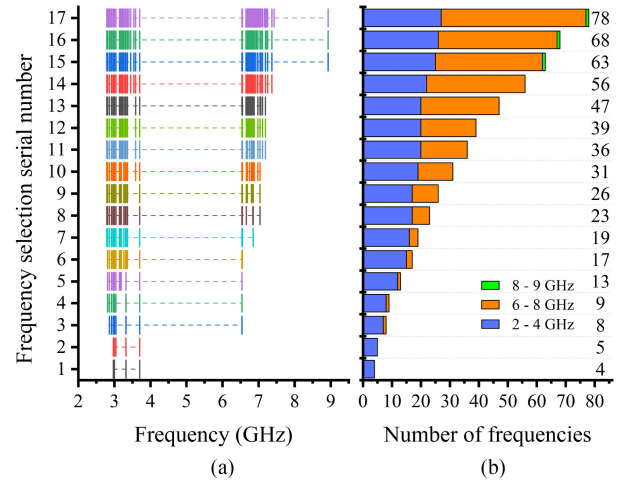


Fig. 8. Candidate frequency subsets generated by the two-stage frequency selection framework. (a) Frequencies distributions of candidate frequency subsets. (b) Proportions of the dominant frequency bands of candidate frequency subsets.

2) Frequency Subset: In the process of frequency selection, the frequency intersection was obtained only when PreNum exceeded 40. Therefore, the frequency selection was performed 20 times, and 17 frequency subsets were obtained. As shown in Fig. 8, the selected frequencies are mainly distributed at 2–4, 6–8, and 8–9 GHz. The lower frequencies (in 2–4 GHz) were selected first, and some higher frequencies were gradually selected with the continuous generation of frequency subsets. The frequencies in the 6–8 and 8–9 GHz bands were selected into frequency subsets starting from frequency subset 3 and frequency subset 15, respectively. The reason for the distribution of selected frequencies may be related to the linearity of the spectrum curves. As shown in Fig. 5(a), the attenuation varies linearly and sharply with the frequency in the 2–4, 6–8, and 8–9 GHz bands, which reveals the difference between those frequencies in the three bands. The RF-RFE algorithm deliberately selects frequencies with different properties into frequency subsets to obtain diverse MC-relevant information. Thus, the selected frequencies are mainly distributed in the three abovementioned bands. The next step involves the selection of the optimal frequency set from these candidate frequency subsets for the OM2S2.

3) Optimal Frequency Set Determined by Voting Strategy: The evaluation of the efficiency of a frequency set involves the assessment of the quality of the model built based on the attenuation and phase shift data corresponding to the frequency set. The k-fold cross-validation method, which is popular for assessing the quality of models, can gauge how well the model generalizes to an independent dataset. In this study, tenfold cross-validation was used to assess regression models because of lower bias and variance, and the metrics applied to evaluate the regression models included the coefficient of determination (R^2), root mean square error (RMSE), and mean absolute error (MAE). As shown in Fig. 9(a) and (b), the R^2 value increases briefly at first and then decreases gradually with the increase in the number of frequencies involved in the frequency set, while

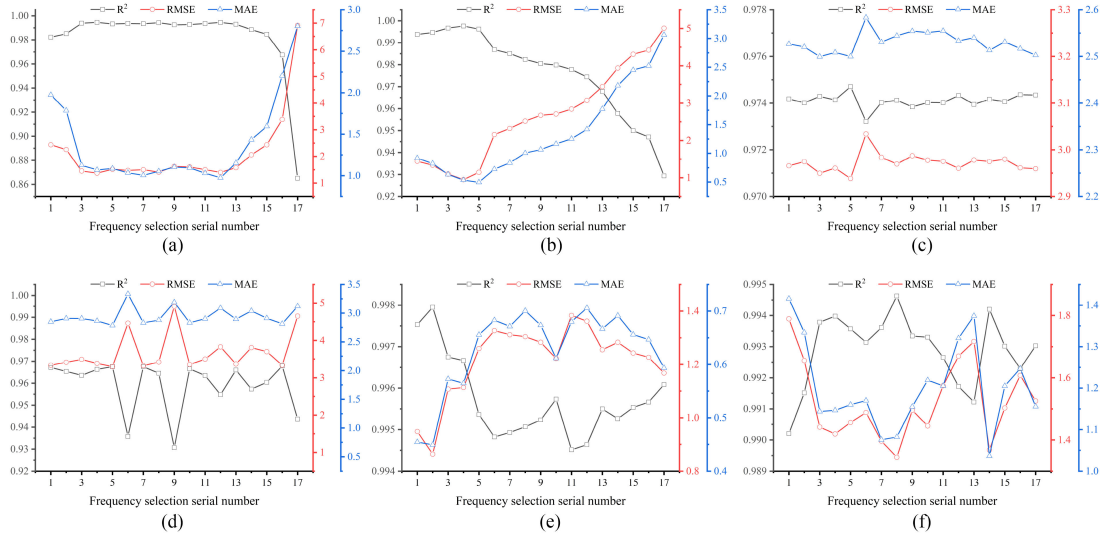


Fig. 9. Cross-validation results of R^2 , RMSE, and MAE. (a) Multiple linear regression (MLR) model. (b) Support vector machine (SVM) model. (c) Random forest model. (d) Adaptive boosting (AdaBoost) model. (e) Extreme gradient boosting (XGBoost) model. (f) Deep neural network (DNN) model.

the RMSE and MAE show opposite trends. As can be seen from Fig. 9(c)–(f), the performance metrics of the RF, AdaBoost, XGBoost, and DNN show a certain fluctuation, while the XGBoost and DNN models have achieved very good performance with higher R^2 value, and lower RMSE and MAE.

The majority voting method (MVM) was used to determine the optimal frequency set according to the results of the tenfold cross-validation. First, the 17 frequency subsets were sorted according to the performance metrics of their corresponding regression models, and the top five frequency subsets were selected. Then, the MVM was used to combine the results of the top five frequency subsets selected by each of the six algorithms, and the frequency subset with the majority votes was selected as the optimal frequency set. The process of selecting the optimal frequency set by MVM can be described as follows:

$$F_{\text{optimal}} = F_{\text{sub}} \arg \max \sum_{j=1}^T h_i^j(x) \quad (7)$$

$$h_i^j(x) = \text{ISIN}(\text{ASN}, \text{SSN}) \quad (8)$$

$$\text{ASN} = \{1, 2, \dots, N\} \quad (9)$$

$$\begin{aligned} \text{SSN} = & \text{INDEX}(\text{LARGEST}(k, \\ & \{\text{METRICS}(i, F_{\text{sub}1}), \dots, \\ & \text{METRICS}(i, F_{\text{sub}j}), \dots, \\ & \text{METRICS}(i, F_{\text{sub}N})\})) \end{aligned} \quad (10)$$

where F_{optimal} is the optimal frequency set, $F_{\text{sub}j}$ is the j th frequency subset, N and T are the number of frequency subsets and regression algorithms, respectively; $\text{METRICS}(i, F_{\text{sub}j})$ calculates the regression metrics of the model established on the data corresponding to $F_{\text{sub}j}$ using the i th algorithm; $\text{LARGEST}()$ selects the top k frequency subsets; $\text{INDEX}()$ searches for the serial numbers of frequency subsets; ASN and SSN are the sets of serial numbers of all frequency subsets and the top k frequency subsets, respectively; $\text{ISIN}()$ calculates the Boolean

TABLE I
PROCEDURE OF MAJORITY VOTING METHOD

Metrics	Models	Frequency subsets					Results
		First	Second	Third	Fourth	Fifth	
R^2	MLR	4 th	12 th	8 th	3 rd	6 th	3 rd
	SVM	4 th	3 rd	5 th	2 nd	1 st	
	RF	5 th	16 th	17 th	12 th	3 rd	
	AdaBoost	16 th	5 th	7 th	1 st	10 th	
	XGBoost	2 nd	1 st	3 rd	4 th	17 th	
	DNN	8 th	14 th	4 th	3 nd	7 th	
RMSE	MLR	4 th	12 th	8 th	3 rd	6 th	3 rd 4 th
	SVM	4 th	3 rd	5 th	2 nd	1 st	
	RF	5 th	3 rd	17 th	12 th	4 th	
	AdaBoost	5 th	7 th	1 st	16 th	10 th	
	XGBoost	2 nd	1 st	3 rd	4 th	17 th	
MAE	DNN	8 th	14 th	7 th	4 th	3 rd	3 rd 4 th
	MLR	12 th	7 th	11 th	6 th	8 th	
	SVM	5 th	4 th	3 rd	6 th	2 nd	
	RF	3 rd	5 th	17 th	4 th	14 th	
	AdaBoost	5 th	16 th	7 th	10 th	1 st	
	XGBoost	2 nd	1 st	4 th	3 rd	17 th	
	DNN	14 th	7 th	8 th	3 rd	4 th	

vector that represents the result of comparison between ASN and SSN; $h_i^j(x)$ is the voting result of the i th algorithm on the j th frequency subset, and x is the original feature data.

As shown in Table I, frequency subset 3 obtained the highest number of votes when the MVM procedure was executed according to R^2 values, while frequency subset 3 and 4 obtained the highest number of votes when the MVM procedure was executed according to RMSE or MAE values. Frequency subset 3 contains eight individual frequencies (2.86, 2.92, 2.97, 3.00, 3.04, 3.32, 3.70, and 6.54 GHz), while frequency subset 4 contains nine individual frequencies (2.81, 2.86, 2.92, 2.97, 3.00, 3.04, 3.32, 3.70, and 6.54 GHz). Although frequency subset 4 has one more frequency (2.81 GHz) than frequency subset 3, the latter received the highest number of votes regardless of which indicator was used in the MVM procedure. In addition,

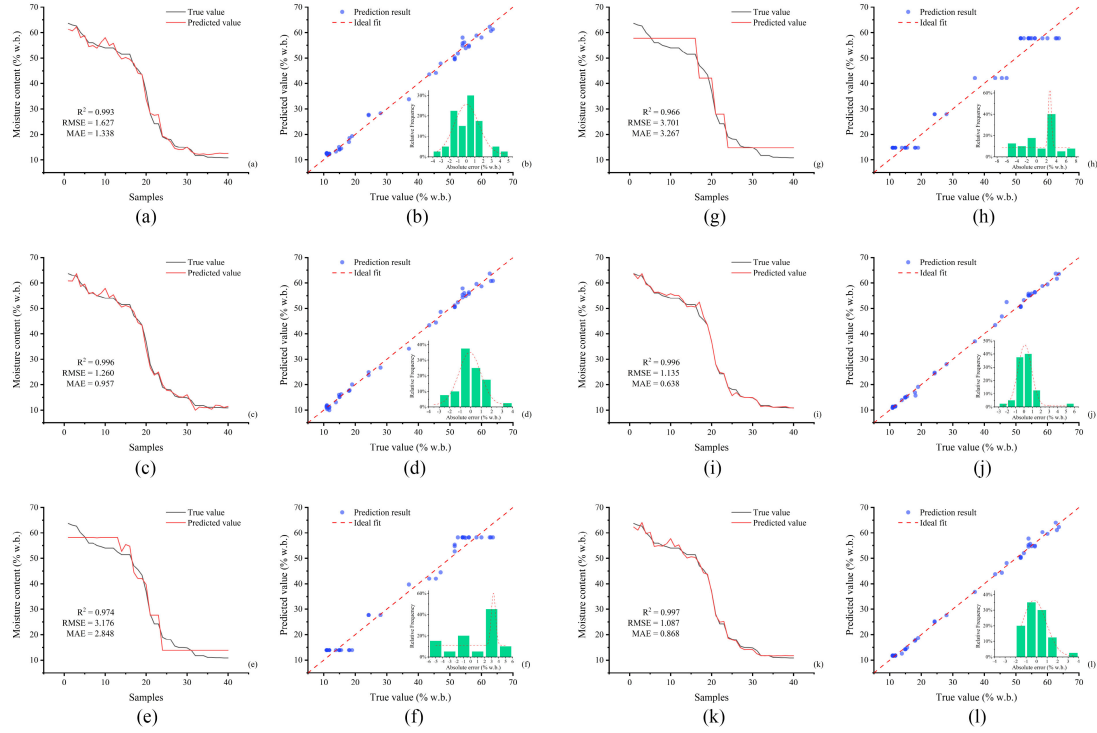


Fig. 10. Prediction results of moisture content by the six models. (a)–(b) Multiple linear regression (MLR) model. (c)–(d) Support vector machine (SVM) model. (e)–(f) Random forest model. (g)–(h) Adaptive boosting (AdaBoost) model. (i)–(j) Extreme gradient boosting (XGBoost) model. (k)–(l) Deep neural network (DNN) model.

using fewer frequencies is conducive for the on-line measurement. Therefore, frequency subset 3 was selected as the optimal frequency set.

C. Prediction Model of Moisture Content

The MC prediction models were developed and validated with the data divided from the original dataset according to frequency subset 3. Fig. 10 presents the curves of the true and predicted MC values; the distribution of prediction errors is also displayed. As shown in Fig. 10(e)–(h), the RF and AdaBoost models do not perform well, and there is no good agreement between the true and predicted MC values. The regression metrics of the RF and AdaBoost models are poor, and the distribution of prediction errors is not quite Gaussian.

The Friedman test and Nemenyi *post hoc* test, which are robust nonparametric methods for statistical comparisons of estimators [30], were used to compare the six algorithms and select the best prediction model. Table II reports the Friedman rankings of the R^2 , RMSE, and MAE obtained with the six algorithms. It can be seen that the DNN achieves the first positions in the R^2 and RMSE rankings, while XGBoost achieves the first position in the MAE ranking. Then the Friedman statistics were calculated as follows:

$$\tau_{\chi^2} = \frac{12N}{k(k+1)} \left(\sum_{i=1}^k r_i^2 - \frac{k(k+1)^2}{4} \right) \quad (11)$$

$$\tau_F = \frac{(N-1)\tau_{\chi^2}}{N(k-1) - \tau_{\chi^2}} \quad (12)$$

TABLE II
FRIEDMAN RANK OF R^2 , RMSE, AND MAE FOR THE SIX MODELS

Pos.	R^2		RMSE		MAE	
	Model	Rank	Model	Rank	Model	Rank
1	DNN	1.0	DNN	1.0	XGBoost	1.0
2	XGBoost	2.5	XGBoost	2.0	DNN	2.0
3	SVM	2.5	SVM	3.0	SVM	3.0
4	MLR	4.0	MLR	4.0	MLR	4.0
5	RF	5.0	RF	5.0	RF	5.0
6	AdaBoost	6.0	AdaBoost	6.0	AdaBoost	6.0

where τ_{χ^2} and τ_F are the original and improved Friedman statistics, respectively; k and N are the numbers of algorithms and datasets, respectively, and r_i is the average rank of the i th algorithm. Because the calculated result of τ_F (77.0) is larger than the critical value for the F test ($F_{0.05} = 2.901$), the null hypothesis, which states that all the algorithms are equivalent, is rejected. Then, the Nemenyi *post hoc* test was used to further distinguish the algorithms, and the critical difference (CD) was calculated as follows:

$$CD = q_\alpha \sqrt{\frac{k(k+1)}{6N}} \quad (13)$$

where critical value $q_\alpha = 2.850$, then the CD was calculated to be 3.77. A heatmap with p -values was plotted to evaluate the performance differences between every two algorithms. As shown in Fig. 11(a), if the color of the rectangle is dark (p -value is small), the difference between the two algorithms is significant. To select the best model, Fig. 11(b) presents the average ranks

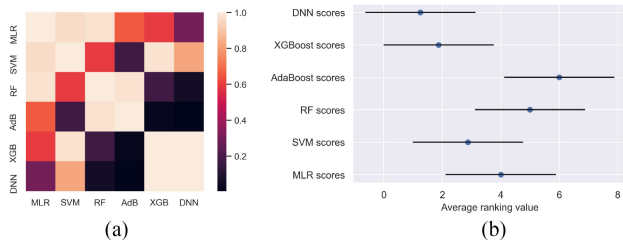


Fig. 11. Comparisons of the six models based on the Friedman test and Nemenyi *post hoc* test. (a) Heatmap with *p*-values to evaluate the performance differences between every two models, a darker rectangle indicates a greater difference between the two corresponding models. (b) Friedman test chart: The blue dots and horizontal segments represent the average ranks and critical difference of the six models; a lower average rank indicates a superior model, the performance of two models is significantly different if the corresponding average ranks differ by at least the critical difference.

TABLE III
MEASUREMENT PERFORMANCE OF OM2S2

Reference (%)	Group 1 ^a (%)	Group 2 ^a (%)	Group 3 ^a (%)	Mean (%)	SD (%)	MAE (%)
63.00	62.26	61.11	63.99	62.45	1.45	1.21
58.42	60.25	56.93	59.60	58.93	1.76	1.50
52.53	53.67	52.06	51.38	52.37	1.18	0.92
45.55	44.34	46.15	44.59	45.03	0.98	0.92
37.43	36.78	37.97	35.92	36.89	1.03	0.90
28.00	27.19	28.95	26.96	27.70	1.09	0.93
24.24	22.92	25.16	24.78	24.29	1.20	0.93
18.18	18.65	16.95	17.17	17.59	0.92	0.90
14.85	13.46	15.82	14.22	14.50	1.20	1.00
11.77	10.67	11.12	12.85	11.55	1.15	0.94

^aGroup 1, Group 2, and Group 3 represent 3 repeated measurements of moisture content.

(represented by blue dots) and the critical difference (represented by horizontal segments) of the six models. If the horizontal segments of any two models do not overlap, it indicates that there is a significant difference between the two models (e.g., see the DNN and AdaBoost). As shown in Fig. 11(b), there is no significant difference between the DNN and other models except the AdaBoost, but the DNN has the smallest average rank (1.25), indicating that it is still superior to the other models. Therefore, the DNN model was deployed in the OM2S2 to measure the MC of unknown samples in real time. To test its overall performance, the OM2S2 was employed to measure the MC of a batch of samples with unknown MC. The measurements at each MC level were repeated three times, and the results of the repeated tests are listed in Table III, corresponding to Group 1, Group 2, and Group 3. To illustrate the accuracy and repeatability of the OM2S2, the mean value, SD, and MAE of the measurement results of the MC are presented in Table III. As shown in Table III, the MAE of the measurements was lower than 1.50% over the entire MC range, indicating that the performance of OM2S2 is acceptable.

V. CONCLUSION

In this study, an OM2S2 was developed to accurately measure the MC of food and agricultural products in a wide range in real time. The main work and conclusions include the following.

- The OM2S2 using a frequency swept signal (ranging from 2.00 to 10.00 GHz) showed acceptable performance for measuring the MC of corn in the range of 10.89–63.64% with a measurement error not more than 1.50% over repeated tests.

2) A two-stage frequency selection framework was presented to optimize the frequency swept signal, and frequency subset 3 (containing eight individual frequencies) was selected as the optimal frequency set from 17 candidate frequency subsets.

- Six algorithms were used to establish MC prediction models, the DNN model ($R^2 = 0.997$, RMSE = 1.087, MAE = 0.868) was selected as the best model by Friedman test and Nemenyi *post hoc* test and deployed to the OM2S2.

In general, the OM2S2 could potentially be applied to highly automated processes in food processing and agriculture-related industries to measure the MC of products in real time. The frequency selection framework offers a complementary strategy for the principle of the selection of the measurement frequency. Furthermore, the adaptability of the OM2S2 and the framework to materials with complex surfaces needs to be further investigated.

REFERENCES

- S. Trabelsi and S. O. Nelson, "Microwave sensing of quality attributes of agricultural and food products," *IEEE Instrum. Meas. Mag.*, vol. 19, no. 1, pp. 36–41, Feb. 2016.
- F. Gardino, B. Montruccchio, M. Rebaudengo, and E. R. Sanchez, "On improving automation by integrating RFID in the traceability management of the agri-food sector," *IEEE Trans. Ind. Electron.*, vol. 56, no. 7, pp. 2357–2365, Jul. 2009.
- K. Staszek, I. Piekarz, J. Sorocki, S. Koryciak, K. Wincza, and S. Gruszcynski, "Low-cost microwave vector system for liquid properties monitoring," *IEEE Trans. Ind. Electron.*, vol. 65, no. 2, pp. 1665–1674, Feb. 2018.
- S. Trabelsi, A. W. Krazewski, and S. O. Nelson, "New density-independent calibration function for microwave sensing of moisture content in particulate materials," *IEEE Trans. Instrum. Meas.*, vol. 47, no. 3, pp. 613–622, Jun. 1998.
- B. Wang, P. Pan, T. P. McDonald, and Y. Wang, "Development of a capacitance sensing system for monitoring moisture content of spray dried gelatin powders," *J. Food Eng.*, vol. 195, pp. 247–254, 2017.
- C. Collell, P. Gou, J. Arnau, I. Muñoz, and J. Comaposada, "NIR technology for on-line determination of superficial Aw and moisture content during the drying process of fermented sausages," *Food Chem.*, vol. 135, no. 3, pp. 1750–1755, 2012.
- P. Clarys, R. Clijnsen, J. Taeymans, and A. O. Barel, "Hydration measurements of the stratum corneum: Comparison between the capacitance method (digital version of the Corneometer cm 825) and the impedance method (Skicon-200 ex)," *Skin Res. Technol.*, vol. 18, no. 3, pp. 316–323, 2012.
- J. Peters *et al.*, "Design, development and method validation of a novel multi-resonance microwave sensor for moisture measurement," *Analytica Chimica Acta*, vol. 961, pp. 119–127, 2017.
- S. Julrat and S. Trabelsi, "Measuring dielectric properties for sensing foreign material in peanuts," *IEEE Sensors J.*, vol. 19, no. 5, pp. 1756–1766, Mar. 2019.
- S. Trabelsi, A. W. Kraszewski, and S. O. Nelson, "A microwave method for on-line determination of bulk density and moisture content of particulate materials," *IEEE Trans. Instrum. Meas.*, vol. 47, no. 1, pp. 127–132, Feb. 1998.
- S. O. Nelson, A. W. Kraszewski, S. Trabelsi, and K. C. Lawrence, "Using cereal grain permittivity for sensing moisture content," *IEEE Trans. Instrum. Meas.*, vol. 49, no. 3, pp. 470–475, Jun. 2000.
- N. Kinayman and M. Aksun, *Modern Microwave Circuits*. Norwood, MA, USA: Artech House, 2005.
- S. O. Nelson and S. Trabelsi, "Historical development of grain moisture measurement and other food quality sensing through electrical properties," *IEEE Instrum. Meas. Magn.*, vol. 19, no. 1, pp. 16–23, Feb. 2016.
- F. Menke and R. Knochel, "New density-independent moisture measurement methods using frequency-swept microwave transmission," in *Proc. IEEE MTT-S Int. Microw. Symp. Dig.*, vol. 3, 1996, pp. 1415–1418.

- [15] S. Okamura and Z. Ma, "Moisture content measurement by microwave attenuation and problems," in *Proc. Int. Conf. Microw. Millimeter Wave Technol.*, 1998, pp. 189–192.
- [16] Z. Ma and S. Okamura, "Analysis and elimination of the reflection influence on microwave attenuation measurement for moisture determination," *IEICE Trans. Electron.*, vol. 80, no. 10, pp. 1324–1329, 1997.
- [17] J. Zhang, D. Du, Y. Bao, J. Wang, and Z. Wei, "Development of multi-frequency swept microwave sensing system for moisture measurement of sweet corn with deep-neural-network," *IEEE Trans. Instrum. Meas.*, vol. 69, no. 9, pp. 6446–6454, Sep. 2020.
- [18] D. Lee, "Nonlinear estimation and multiple sensor fusion using unscented information filtering," *IEEE Signal Process. Lett.*, vol. 15, pp. 861–864, Dec. 2008.
- [19] T. Loutas, N. Eleftheroglou, G. Georgoulas, P. Loukopoulos, D. Mba, and I. Bennett, "Valve failure prognostics in reciprocating compressors utilizing temperature measurements, PCA-based data fusion, and probabilistic algorithms," *IEEE Trans. Ind. Electron.*, vol. 67, no. 6, pp. 5022–5029, Jun. 2020.
- [20] Y. LeCun, Y. Bengio, and G. Hinton, "Deep learning," *Nature*, vol. 521, no. 7553, p. 436, 2015.
- [21] O. Costilla-Reyes, P. Scully, and K. B. Ozanyan, "Deep neural networks for learning spatio-temporal features from tomography sensors," *IEEE Trans. Ind. Electron.*, vol. 65, no. 1, pp. 645–653, Jan. 2018.
- [22] S. Taheri, G. Brodie, M. V. Jacob, and E. Antunes, "Dielectric properties of chickpea, red and green lentil in the microwave frequency range as a function of temperature and moisture content," *J. Microw. Power Electromagn. Energy*, vol. 52, no. 3, pp. 198–214, 2018.
- [23] S. Trabelsi, A. W. Kraszewski, and S. O. Nelson, "Phase-shift ambiguity in microwave dielectric properties measurements," *IEEE Trans. Instrum. Meas.*, vol. 49, no. 1, pp. 56–60, Feb. 2000.
- [24] *Gb 5009.3–2016 Determination of Moisture Content in Food, NHFPC, GB 5009.3-2016*, 2016. [Online]. Available: <https://sppt.cfsa.net.cn:8086/staticPages/7BD4B017-E834-4EC8-A126-D2FABA88DFDA.html>
- [25] P. M. Granitto, C. Furlanello, F. Biasioli, and F. Gasperi, "Recursive feature elimination with random forest for PTR-MS analysis of agroindustrial products," *Chemometrics Intell. Lab. Syst.*, vol. 83, no. 2, pp. 83–90, 2006.
- [26] M. Kang, M. R. Islam, J. Kim, J. Kim, and M. Pecht, "A hybrid feature selection scheme for reducing diagnostic performance deterioration caused by outliers in data-driven diagnostics," *IEEE Trans. Ind. Electron.*, vol. 63, no. 5, pp. 3299–3310, May 2016.
- [27] B. F. Darst, K. C. Malecki, and C. D. Engelman, "Using recursive feature elimination in random forest to account for correlated variables in high dimensional data," *BMC Genetics*, vol. 19, no. 1, 2018, Art. no. 65.
- [28] Q. Chen, Z. Meng, X. Liu, Q. Jin, and R. Su, "Decision variants for the automatic determination of optimal feature subset in RF-RFE," *Genes*, vol. 9, no. 6, 2018, Art. no. 301.
- [29] L. Lam and S. Y. Suen, "Application of majority voting to pattern recognition: An analysis of its behavior and performance," *IEEE Trans. Syst. Man, Cybern. - Part A: Syst. Humans*, vol. 27, no. 5, pp. 553–568, Sep. 1997.
- [30] J. Demšar, "Statistical comparisons of classifiers over multiple data sets," *J. Mach. Learn. Res.*, vol. 7, pp. 1–30, Jan. 2006.



Jinyang Zhang (Student Member, IEEE) received the B.S. degree in agricultural mechanization and automation from Northwest A&F University, Yangling, China, in 2017. Since 2017, he has been working toward the Ph.D. degree in agricultural mechanization engineering with Zhejiang University, Hangzhou, China.
His current research interests include the application of microwave technique, development of online detection equipment, and moisture content measurement. He is a member of IEEE Industrial Electronics Society.



Yin Bao received the B.S. degree in mechanical (vehicle) engineering from China Agricultural University, Beijing, China, in 2012, and the Ph.D. degree in agricultural and biosystems engineering from Iowa State University, Ames, IA, USA, in 2018.

From May 2018 to August 2019, he continued his research work in the Agricultural and Biosystems Engineering Department, Iowa State University, Ames, IA, USA, as a Postdoctoral Research Associate. Since August 2019, he has been an Assistant Professor with the Biosystems Engineering Department, Auburn University, Auburn, AL, USA. His current research interests include precision agriculture and forestry, cyber-physical systems, remote and proximal sensing, machine learning, and computer vision and robotics.



Dongdong Du received the Ph.D. degree in agricultural engineering from Zhejiang University, Hangzhou, China, in 2017.

He is currently an Assistant Research Fellow with the College of Biosystems Engineering and Food Science, Zhejiang University. His current research interests include intelligent agricultural equipment and signal processing.



Jun Wang received the B.S. degree in agricultural engineering, the M.S. degree in engineering properties from Zhejiang Agricultural University, Hangzhou, China, in 1986 and 1991, respectively.

He has been working with Zhejiang University, Hangzhou, China, since 1998, where he has been a Professor, since 1999. His research interests include engineering properties of agricultural materials, detection food quality by E-nose and E-tongue, and agricultural equipment.



Zhenbo Wei (Member, IEEE) received the B.S. and M.S. degrees from Hebei Agricultural University, Baoding, China, in 2005 and 2007, and the Ph.D. degree from Zhejiang University, Hangzhou, China, in 2011, all in agricultural engineering.

He continued his research with Zhejiang University as a Postdoctoral Research Associate, in 2011. He is currently an Associate Professor of College of Biosystems Engineering and Food Science, and Vice-Chair of BE Department with Zhejiang University. His research interests include nondestructive testing technology for internal quality of biological materials and smart agriculture.